

www.acsami.org Research Article

Revealing the Grain-Boundary-Cracking Induced Capacity Decay of a High-Voltage LiCoO₂ at 4.6 V

Haocong Yi, Yuhao Du, Jianjun Fang, Zijian Li, Hengyu Ren, Wenguang Zhao, Hui Chen,* Lin Zhou, Qinghe Zhao,* and Feng Pan*



Cite This: ACS Appl. Mater. Interfaces 2023, 15, 42667–42675



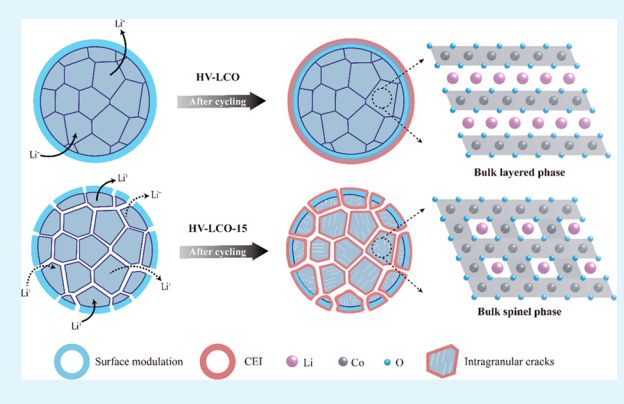
ACCESS I

Metrics & More

Article Recommendations

Supporting Information

ABSTRACT: During a practical battery manufacture process, the LiCoO₂ (LCO) electrodes are usually rolled with high pressure to achieve better performance, including reducing electrode polarization, increasing compact density, enhancing mechanical toughness, etc. In this work, a high-voltage LCO (HV-LCO) is achieved via modulating a commercialized LCO with an Al/F enriched and spinel reinforced surface structure. We reveal that the rolling can more or less introduce risk of grain-boundary-cracking (GBC) inside the HV-LCO and accelerate the capacity decay when cycled at 3-4.6 V vs Li/Li⁺. In particular, the concept of interface structure is proposed to explain the reason for the deteriorated cycle stability. As the GBC is generated, the interface structure of HV-LCO alters from a surface spinel phase to a hybrid of surface spinel plus boundary layer phases, leading to the exposure of some the nonprotective layer phase against the electrolyte.



This alternation causes serious bulk structure damage upon cycles, including expanding GBC among the primary crystals, forming intragranular cracks and inactive spinel phases inside the bulk regions, etc., eventually leading to the deteriorated cycle stability. Above all, we realize that it is far from enough to achieve a eligible high-voltage LCO via only applying surface modification. This work provides a new insight for developing more advanced LCO cathodes.

KEYWORDS: LiCoO₂, Interface structure, Grain-boundary-cracking, Capacity decline, Practical applications

1. INTRODUCTION

Among the reported cathode materials, LiCoO₂ (LCO) has long dominated the consumer battery market due to its high volumetric energy density, easy production, and excellent reliability. For industry, the steps seeking better batteries with higher energy density never stop, aiming to achieve longer usage time. Nowadays, the commercialized LCO/graphite batteries with upper charge voltage of 4.45 V/4.48 V have already supplied in large quantities, with discharge capacities of about 180 to 190 mAh g⁻¹. ²⁻⁴ Once further pushing the upper charge voltage of the full batteries to 4.55 V, corresponding to 4.6 V vs Li/Li+, the available discharge capacity of LCO is expected to beyond 215 mAh g⁻¹, which is an extremely appealing capacity release and shows a promising economic value for industry.^{5,6} However, the reason for structural instability of LCO remains vague, which restricts the further development of the high-voltage LCO.

In recent years, lots of the researchers have paid much attention to develop the high-voltage LCO cycling at 4.6 V. The previous reports of our team show that, the curvature of the cobalt oxide layers nearby the surface region dominates the structural stability of LCO at high potentials,7 and in turn, the electrode performances. Based on this basis, we have

developed some facile methods to reinforce the surface structure of LCO, including reconstructing an Al/F enriched and spinel reinforced surface to reduce the side reaction,8 and promoting the surface electric conductivity of LCO by over one magnitude via constructing a disordered rock-salt phase in the surface region. Besides, we also have developed a one-step sintering synthesis to achieve a combination of bulk Li/Co antisites, Mg-pillar enriched surface, and thin Mg-O coating layer for enhanced structure stability in both the bulk and surface region. 10

Meanwhile, similar surface modulation strategies have also been reported by other groups. For example, Huang's group reported a Zr-doped and Li⁺ conductive Li₂Zr(PO₄)₂ interspersed LiCoO2, facilitating to form a durable CEI with strong stability and low interface resistance. 11 Yang's group revealed a lattice-matched LiCoPO4 coating on LCO, which

Received: June 23, 2023 Accepted: August 21, 2023 Published: August 28, 2023





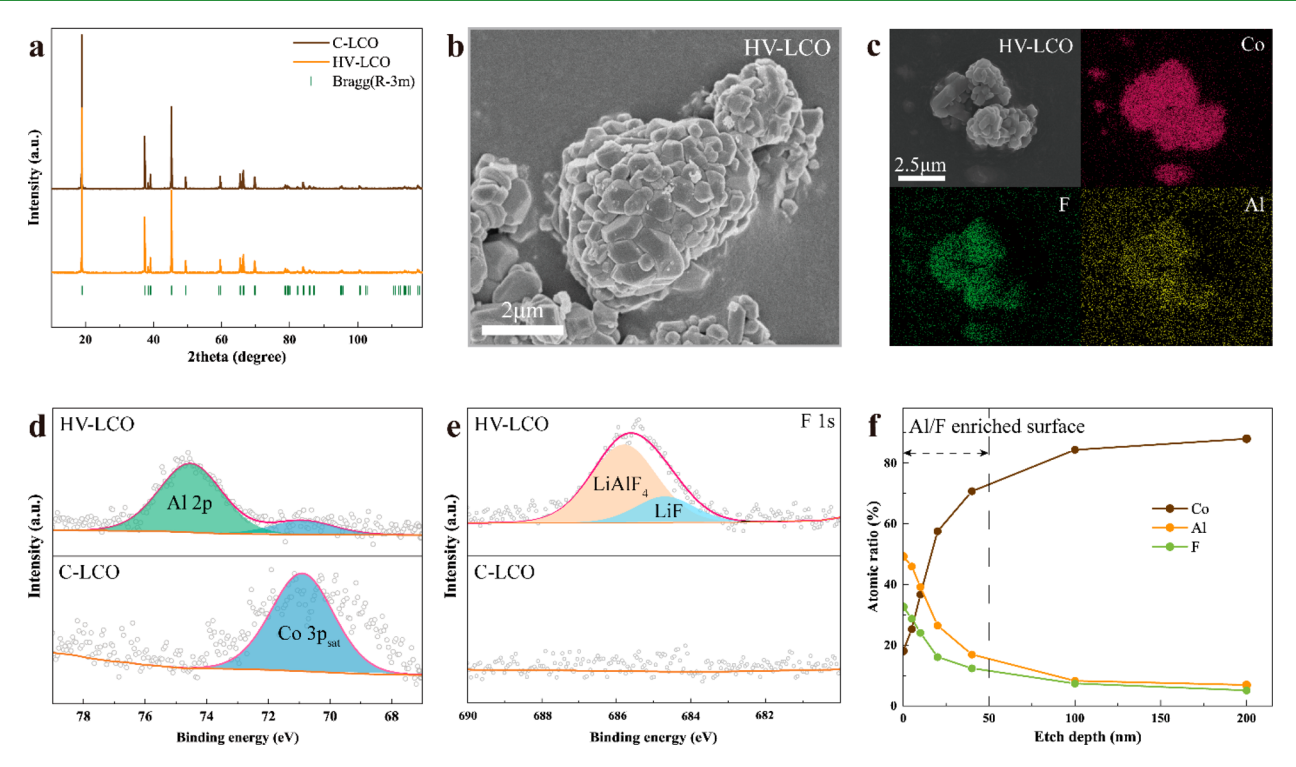


Figure 1. Material characterizations of the high-voltage LCO. (a) XRD patterns of the C-LCO and HV-LCO, (b) SEM morphology, and (c) EDS-mapping results of Co, Al, and F elements of HV-LCO. XPS analyses of the (d) Al and (e) F elements on the surface of HV-LCO and (f) in-depth distribution of the Al, F, and Co elements from surface to interior.

ensured a stable CEI with fewer side reactions, and reduced phase collapse upon cycling at 4.6 V (vs Li/Li⁺) or above. Fan et al. proposed a RbAlF₄ modified LCO, which demonstrated a high capacity of >220 mAh g⁻¹ and impressive retention of >80/77% after 500/300 cycles at 30/45 °C. ¹³ Lu's group attempted multiple strategies, including Li–Al–F coating, ¹⁴ Li–Al–PO₄ coating, ¹⁵ LiF and Li₂CoTi₃O₈ surface modifications, ¹⁶ etc. to obtained enhanced cycle stability of LCO at 4.6 V. Li's group developed a high-voltage LCO via constructing a semicoherent LiMn_{1.5}Ni_{0.5}O₄ spinel surface shell, which prevented oxygen release and enhanced hybrid anion- and cation-redox reversibility at 4.6 V or above. ¹⁷

Despite the great advances, the optimization effects of the above reports belong to a "lab-level" evaluations, and are mainly concentrated on the surface modulation. In a practical manufacturing process, the requirements for an eligible LCO are more complicated. Some significant differences between the lab and practical conditions mainly focus on the rolling process, the ratio of active materials in electrodes, the electrolyte content, etc. ^{18,19} In particular, the rolling pressure in practical can reach a high value of >10 MPa, much larger than that in lab condition (<2 MPa). Under such a high roll pressure, the active particles face a risk of forming cracks, ^{20,21} in turn, adversely affects the electrode performance, just like the circumstances in this work.

Previously, researchers focused mainly on the crack generation in the layered materials upon cycle. For example, Jiang et al. investigated the cracking mechanism at a coherent grain boundary of LCO, and identified the two kind of cracks as cleavage crack and decomposition crack. Yan et al. reported the nucleation and growth of intragranular cracks in $\text{LiNi}_{1/3}\text{Mn}_{1/3}\text{Co}_{1/3}\text{O}_2$, and found the generation of intragranular cracks is directly associated with high-voltage cycling. Yaqoob et al. revealed that the delithiation-induced

formation of oxygen vacancy was attributed to the generation of microcracking inside LiCoO₂ upon high-voltage cycling. Jun's group found that the nanocrack formation was related with both the mechanical properties and the local deficiency in Li ions under a overcharging condition. Tang's group further reported a strong particle size dependence in both the nucleation and growth of cracks, and revealed that the high-voltage cycle can trigger much more pronounced crack growth. As clarified above, the previous reports mainly analyzed the crack formation in layered materials upon a high-voltage cycle or in overcharge condition. However, the practical rolling process may introduce some prefabricated cracks inside the LCO particle, and the influence of this kind of crack is rarely reported.

Herein, we demonstrate the grain-boundary-cracking (GBC) induced capacity decay of a high-voltage LCO at 4.6 V. We successfully synthesize a high-voltage LCO via modulating a commercialized LCO with an Al/F enriched and spinel reinforced surface structure. For the rolled electrode, we observe obvious GBC generation inside the active particles, which is closely correlated with the deteriorated cycle stability. The concept of interface structure is introduced to explain the reason for the deteriorated cycle stability of the rolled electrodes. We reveal that for a high-voltage LCO without rolling the interface structure just refers to the surface spinel phase, while for the rolled one the interface structure includes both the surface spinel phase and the boundary layer phase. The altered interface structure causes serious bulk structure damage upon cycles due to the exposure of nonprotective layer phase against the electrolyte, leading to the deteriorated cycle stability. This result indicates that an eligible high-voltage LCO can be hardly achieved via only applying the surface modification and provides some constructive perspectives for developing more advanced high-voltage LCO.

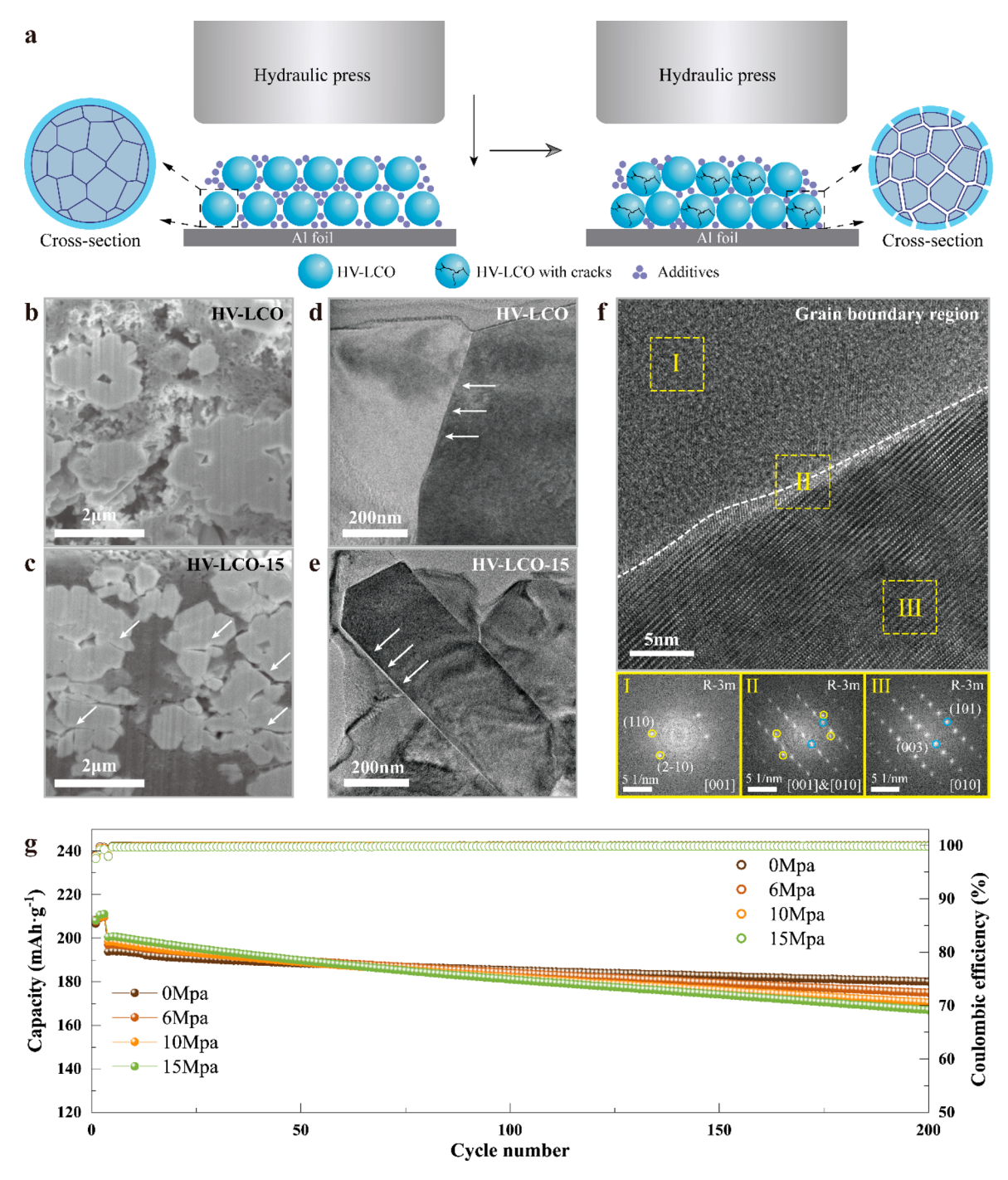


Figure 2. The GBC generation under high pressure. (a) Schematic diagram for the GBC generation inside the rolled HV-LCO. (b, c) The cross-section morphology of HV-LCO and HV-LCO-15 electrodes. (d, e) TEM cross-section morphology of HV-LCO and HV-LCO-15 particles. (f) TEM characterization of the grain boundary of HV-LCO and corresponding diffraction patterns in selected regions. (g) Comparison of the cycle stability curves of HV-LCO electrodes rolled under different pressures.

2. EXPERIMENTAL SECTION

2.1. Material Synthesis. Commercialized LCO (C-LCO) powders are purchased from Pulead Technology Industry Co., Ltd. (China). HV-LCO is prepared by a wet-coating process. First, 100 mmol C-LCO, 4 mmol Al(NO₃) $_3$ ·9H $_2$ O (99%, Aladdin), and 12 mmol NH $_4$ F (99%, Aladdin) are dispersed, stirred for 10 h in a deionized water, and then continuously stirred to dry at 80 °C. Then, the obtained composite is sintered at 500 °C in a Ar atmosphere for 10 h to obtain the HV-LCO.

2.2. Electrochemical Test. The C-LCO and HV-LCO electrodes are prepared by mixing C-LCO or HV-LCO powder, carbon black,

and PVDF (99%, Aladdin) in *N*-methyl-1,2-pyrrolidone (NMP, 99%, Aladdin) to a homogeneous slurry. The mass ratio of LCO: carbon black: PVDF is 8:1:1 in weight. The slurry is then cast onto aluminum foil with a blade and dried at 120 °C in a vacuum oven for 12 h. The mass loading of active material is about 6 mg/cm². HV-LCO electrodes are rolled at different pressure (0–15 MPa) via a manual hydraulic press machine. 2032-type coin cells are assembled in an argon-filled glovebox with LiCoO₂ materials as the cathode, lithium foil as the anode, Celgard film as the separator, and 1.0 M LiPF₆ in ethyl carbonate/ethyl methyl carbonate/fluoroethylene carbonate (EC/EMC/FEC) as the electrolyte. The charge—discharge performance is carried out in the NEWARE battery test system at 25 °C. To

analyze the long-term cyclability, the coin cells are charged and discharged at 1 C (1 C = 200 mAh $\rm g^{-1}$) for 200 cycles. The cyclic voltammetry (CV) is performed on the Solartron Analylical 1470E electrochemical workstation in a potential range of 3–4.6 V, and with a scan rate of 0.2 mV $\rm s^{-1}$.

2.3. Material Characterizations. The crystal structure of samples is analyzed by XRD using a Bruker D8 Advance diffractometer with a Cu-K α radiation source (λ = 0.154 nm). Rietveld refinements of XRD patterns are performed using the FullProf suite. Morphology and elemental distribution investigations of the samples are conducted using a scanning electron microscope (SEM, Zeiss SUPRA-55) with a X-Max EDS detector. The crosssection samples are prepared by Ion Beam Slope Cutter (Leica EM TIC 3X). The transmission electron microscope (TEM) is collected on a field-emission transmission electron microscope (FETEM, JEOL-3200FS) operating at an accelerating voltage of 300 kV with a 60 cm camera length, with a minimum collection angle of -30° to 30°, and a OneView CMOS camera (Gatan Inc.). TEM samples are prepared using the Focus ion beam (FIB). The chemical states of the selected elements are investigated by X-ray photoelectron spectrometry (XPS) on a Thermo Scientific Escalab 250Xi spectrometer.

3. RESULTS AND DISCUSSION

3.1. Characterizations of a High-Voltage LCO. The high-voltage LCO (HV-LCO) is obtained via modulating the surface structure of a commercialized LCO (C-LCO), i.e., forming an Al/F enriched and spinel reinforced surface structure, which has been proved to be effective to enhance the cycle stability of LCO at 4.6 V vs Li/Li⁺.8,9 The synthesis of HV-LCO is achieved via a simple wet-coating process, followed by high-temperature annealing. The phase structures of C-LCO and HV-LCO ire tested by X-ray diffraction (XRD), all the characteristic XRD peaks are well indexed to a typical layered LiCoO₂ phase (Figure 1a). Further XRD refinements show nearly the same lattice parameters of two samples, indicating that the surface modification has little influence on the bulk structures of LCO (Figure S1). Figure 1b shows the surface morphology of HV-LCO, which remains nearly unchanged before and after surface modulation (Figure S2). Meanwhile, the corresponding SEM EDS-mapping results in Figure 1c show the homogeneous distribution of Al and F on the HV-LCO surface. X-ray photoelectron spectroscopy (XPS) results demonstrate the existence of obvious Al/F signals (Figure 1d, 1e).²⁷ Furthermore, the in-depth analyses of Al/F at the near-surface region show that the thickness of the Al/Fenriched layer is about 50 nm (Figures 1f, S3).

To analyze the surface structures of HV-LCO, transmission electron microscopy (TEM) and corresponding diffraction patterns are utilized (Figure S4). The results clearly reveal that, the modulated surface in region A (the outermost surface) is featured with a spinel phase, with a thickness of about 5 nm. We consider that the Al/F enrichment promotes the generation of thin surface spinel phase layer, which is thermodynamically more stable than the layered phase, and plays a significant role on suppressing the surface structure collapse under high-voltage operation. Similar to the previous reports, both the surface Al/F enrichment and surface spinel phase layer benefits for the enhanced cycle stability, via stabilizing the lattice structure, ^{28–30} suppressing the side reaction, ^{31,32} as well as depressing the oxidative oxygen redox,³³ etc. Besides, the bulk regions B and C still remain in the layered phase, hinting that the surface modulation has little influence on the bulk structure. Therefore, we have successfully synthesized the HV-LCO, stabilizing with an Al/F enriched and spinel reinforced surface structure. Further

comparison of the cycle stability curves at 1C current is shown in Figure S5. The HV-LCO shows obviously enhanced cycle stability compared with C-LCO, demonstrating a significant optimization effect of surface modulation against the high-voltage cycle.

3.2. Formation of Grain-Boundary-Cracking. Despite the beneficial effect of surface modulation, the cycle stability of the rolled HV-LCO remains ambiguous. In practical applications, the rolling process is usually a required step to promote the electric property, to increase the compact density and to enhance the mechanical toughness of electrode, etc. In a laboratory condition, the rolling process of electrodes are achieved via a manual hydraulic press machine (Figure S6), and the applied pressure increases gradually from 0 to 15 MPa. The corresponding schematic diagram to clarify this process is shown in Figure 2a. After rolling, the compact density of the electrode increases gradually upon the increased roll pressure (Figure S7), hinting at the increased volumetric energy density.

Another side we do not want to see is that applying the rolling process may introduce the risk of forming cracks inside HV-LCO. To identify the crack's generation, the electrodes without rolling (HV-LCO) and rolled at 15 MPa (HV-LCO-15) are selected. First, from a macroscopic view in SEM results in Figure S8, the HV-LCO-15 shows obvious cracks, while for HV-LCO, no visible cracks appears. We further realize that the cracks grow mainly along the grain boundaries of HV-LCO, thus we name it grain-boundary-cracking (GBC). Meanwhile, the cross-sectional morphology of the electrodes are further presented in Figure 2b, 2c. It is observed that no GBC appears inside the HV-LCO, while obvious GBC is observed inside HV-LCO-15. In particular, the length of GBC in HV-LCO-15 is observed to be beyond 1 μ m. At this macroscopic scale of length, the electrolyte penetration inevitably occurs along the GBC of HV-LCO, which is responsible for the deteriorated cycle stability at 4.6 V.

TEM is further applied to monitor the GBC at a more microscopic scale, as demonstrated in Figure 2d, 2e. For the HV-LCO without rolling, the primary crystals are tightly bonded together via grain boundaries. However, for HV-LCO-15 rolled at 15 MPa, obvious GBC grows along the grain boundaries. That is to say, for HV-LCO, applying the roll process is accompanied more or less with the generation of GBC, which is a very noteworthy issue for industrial production. To clarify the essence for the GBC generation, TEM analyses is further utilized (Figure 2f). The results show that the grain boundary located in the interface region among the primary crystals shows the same layered structure but with different orientations, as confirmed by the diffraction patterns in regions I to III, which inevitably lead to the lattice disorder in the grain boundary region to facilitate the GBC generation under high roll pressure.

The GBC generation greatly affects the electrode performances. The cycle stability curves (at current of 1C) of HV-LCO electrodes rolled under different pressures are presented in Figure 2g. With increasing roll pressure, the discharge capacity gains gradually, while the capacity decline becomes worse gradually. One can imagine that increasing the roll pressure can elevate the electric conductivity of electrode to promote the capacity release, while the roll-induced GBC contributes mainly to the deteriorated cycle stability. The charge/discharge curves, especially in the first cycle, provides more clues for this result, as shown in Figure S9. Comparing the first charge curves, we observe that the charge polarization decreases

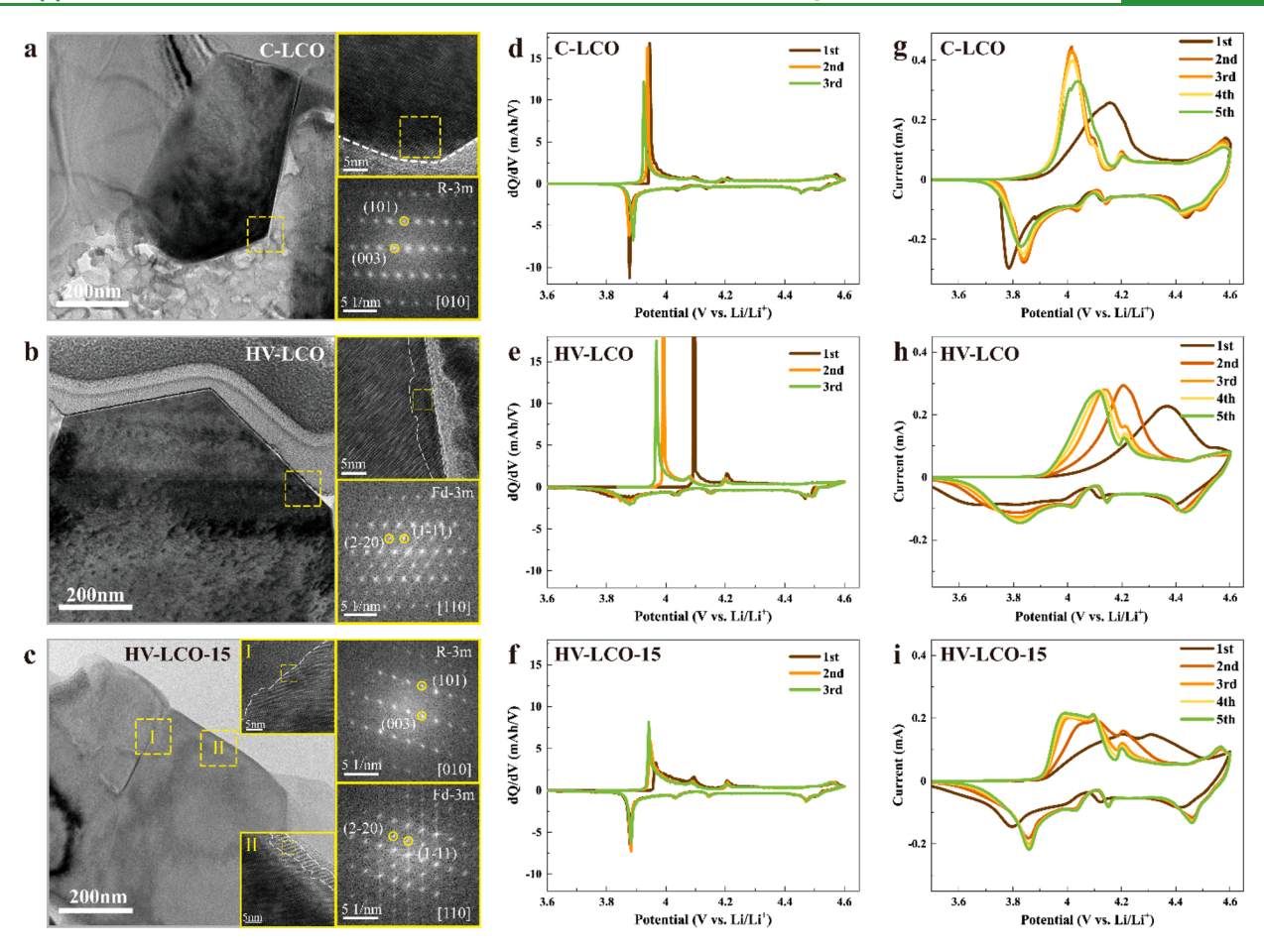


Figure 3. Correlations between interface structures and Li⁺transport routes. (a-c) TEM characterizations and corresponding diffraction patterns in selected regions of C-LCO, HV-LCO, and HV-LCO-15. (d-f) dQ/dV curves in initial 3 cycles of C-LCO, HV-LCO, and HV-LCO-15. (g-i) CV curves in initial 5 cycles of C-LCO, HV-LCO, and HV-LCO-15.

gradually as increasing the roll pressure from 0 to 15 MPa. We deduce that there are two reasons for this decreased polarization: one is the enhanced electric conductivity of the electrode, and the other is the altered interface structure for Li⁺ transport owing to the GBC generation rolled under higher pressure. The detailed correlation between the electrode performances and GBC generation will be discussed in the following part.

3.3. Altered Li⁺ **Transport Routes.** Generally, for cathode materials, there is a close correlation between the structure and electrode performance, especially the structure of interface region which directly contacts with the electrolyte. 34,35 Herein, we find that there exists significant difference among the interface structures of the samples, including C-LCO, HV-LCO, and HV-LCO-15, as demonstrated by the TEM and correlated diffraction pattern results in Figure 3a to 3c. For C-LCO and HV-LCO without GBC, the interface structures just refers to the surface structures, showing a pure layered phase and a pure spinel phase, respectively. However, for HV-LCO-15 rolled with a pressure of 15 MPa, the interface structure includes both the surface spinel phase and the layered phase nearby the GBC, i.e., exhibiting hybrid interface structures with layer plus spinel phases. The difference among interface structure of samples inevitably leads to the differences in cycle stability, which is ordered from high to low as HV-LCO > HV-LCO-15 > C-LCO. In essence, the alternation of interface structure due to the GBC generation is the root cause for the deteriorated cycle performance of the rolled HV-LCO electrodes.

The dQ/dV curves are further applied to explore the influence of altered interface structure on the electrode behaviors, as shown in Figure 3d to 3f. The plateau potential for Li+ extraction across the interface structure during the charge process can be obtained from the current peaks of the dQ/dV curves. The higher the plateau potential, the more difficult the Li⁺ extraction. It can be seen that, the values of plateau potential in initial three cycles are 3.948, 3.938, and 3.926 V for C-LCO, are 4.093, 3.991, and 3.968 V for HV-LCO, and are 3.965, 3.949, and 3.940 V for HV-LCO-15, respectively. The results indicate that the difficulty of Li+ extraction across interface structures is ordered as follows: the pure spinel phase of HV-LCO > the hybrid phases of the layer plus spinel of HV-LCO-15 > the pure layer phase of C-LCO, which is positively correlated with the gradually decreased cycle stability. In other words, the durability of the spinel-type interface structure against the repeated Li⁺ extraction/insertion is much better than the layer-type interface structure. The GBC introduces additional layer-type interface structure in HVM-LCO-15, which is the structure origin for the deteriorated cycle stability. Besides, it is worth noting that the current peak of HV-LCO representing the discharge plateau potential does not appear until the fifth cycle (Figure S10), demonstrating a gradual activation behavior of the spinel-type interface structure upon cycle. The results also

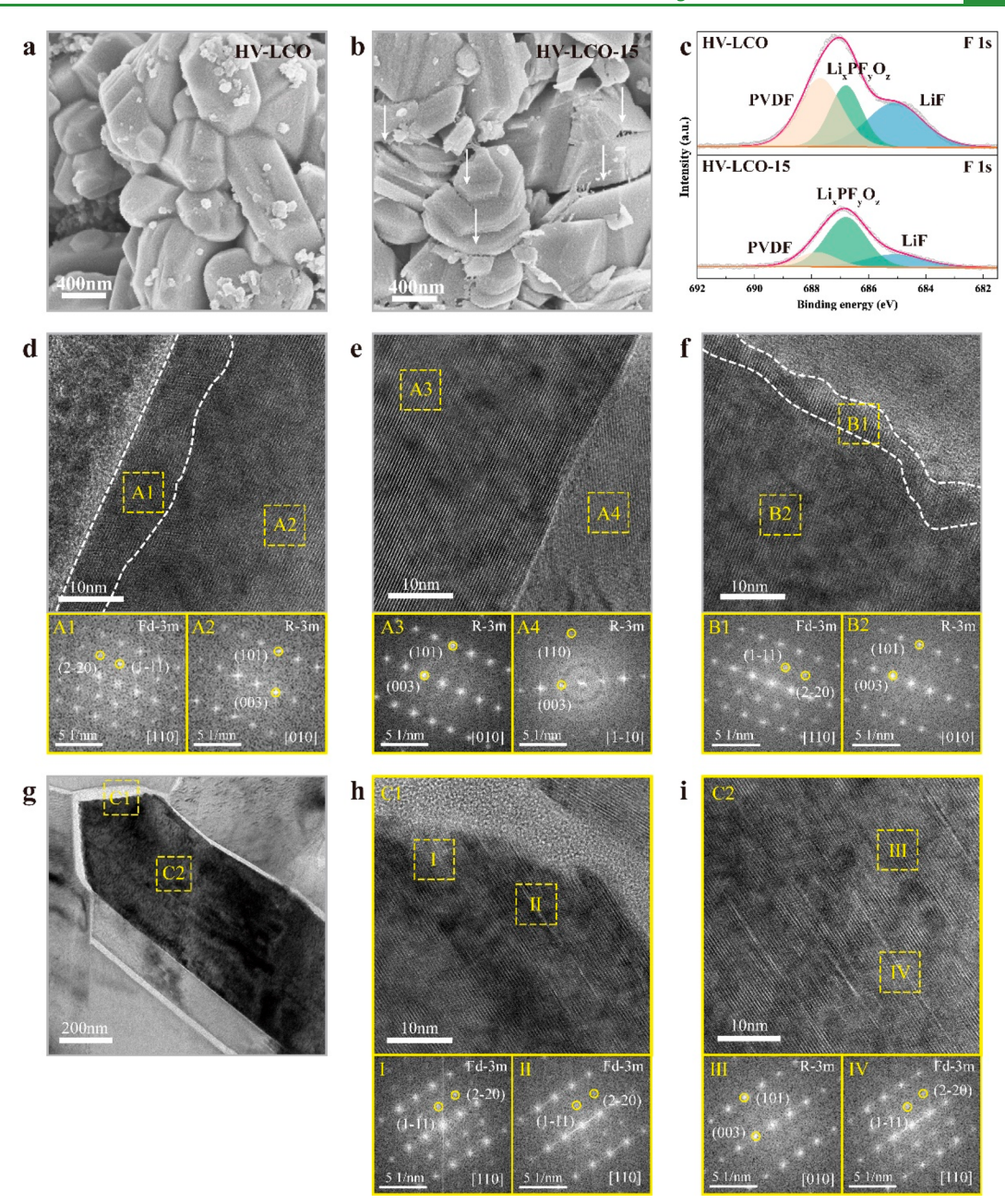


Figure 4. Material characterization after 200 cycles at a current of 1C. (a, b) SEM morphology of HV-LCO and HV-LCO-15. (c) Comparison of XPS F 1s spectra results. (d, e) TEM results of HV-LCO and corresponding diffraction patterns. TEM results of HV-LCO-15 in the surface region (f) and nearby the GBC region (g, h, i) and the corresponding diffraction patterns.

demonstrate that, if the pristine interface structure of a LCO cathode includes some layer-type phase, there exists a risk of fast capacity decline, which can be considered as an index for evaluating the high-voltage LiCoO₂.

We further applied the cyclic voltammetry (CV) curves to reveal the influence of interface structure alternation due to GBC generation. Unlike the $\mathrm{d}Q/\mathrm{d}V$ curves, the CV curves mainly characterizes the Li⁺ extraction/insertion behavior nearby the surface region, and the depth of this surface region fluctuates from tens to hundreds of nanometers based on the scanning speed considerations. Figure 3g to 3i shows the CV curves of three kinds of samples in the initial 5 cycles, with a scan rate of 0.2 mV s⁻¹ and in range of 3.0–4.6 V. Upon charging, we find that the redox peaks shift gradually from high potential to lower potentials in the initial 5 cycles and stabilize

after the fourth cycle. Thus, the CV curves after the fourth cycle are compared to reveal the influence of GBC on dQ/dV curves. The stabilized CV curves show a single redox peak for C-LCO and HV-LCO with potential of 4.016 and 4.109 V, corresponding to the Li⁺ extraction potential from layer-type and spinel-type structures, respectively. Interestingly, we further find that, for HV-LCO-15, the redox peaks are separated into two peaks with potentials of 3.998 and 4.091 V, mainly due to a hybrid Li⁺ extraction from interface structures of both layered and spinel phases. The comparison of CV curves further verifies the alternation of Li⁺ transport routes due to the GBC generation. Based on the above results, it is believed that the GBC can introduce layer-type interface structure in HV-LCO. When this layer-type interface structure is exposed to the electrolyte, the Li⁺ transport routes is varied,

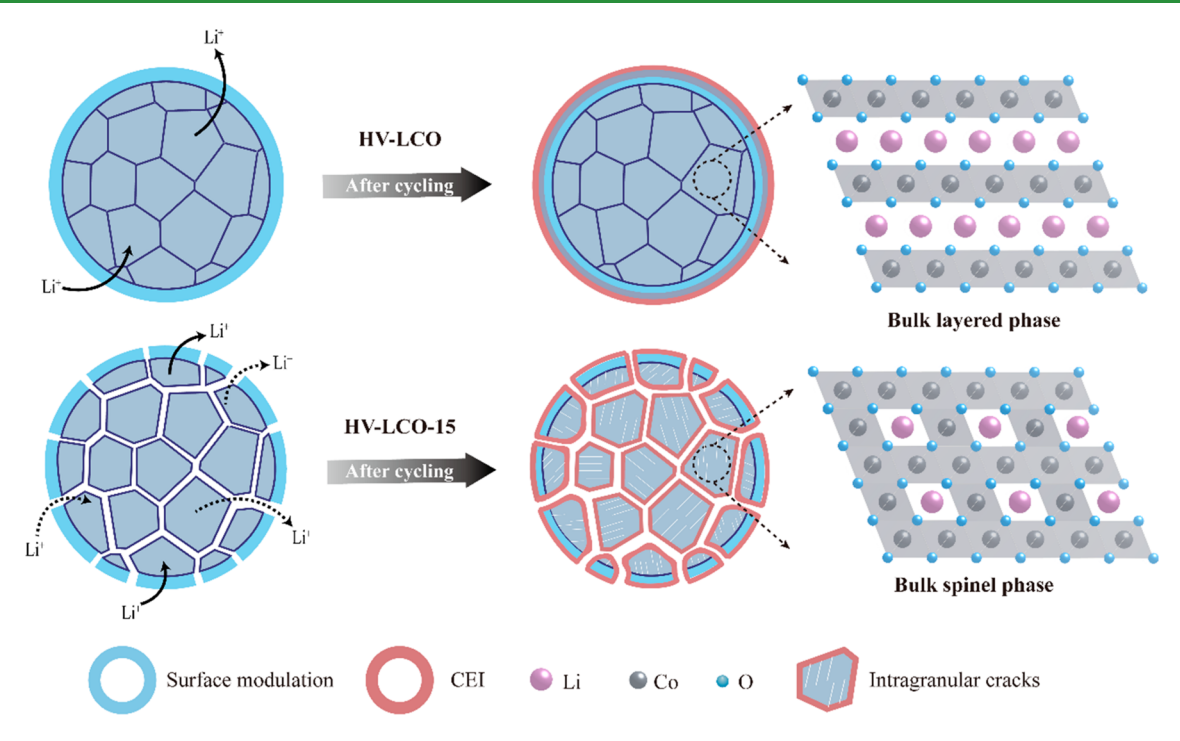


Figure 5. Schematic diagram of the GBC induced capacity decline by comparing HV-LCO and HV-LCO-15.

thereby affecting the cycle stability at 4.6 V. Besides, the GBC generation also affects the side reactions, which causes more decomposition of both solvents and LiPF $_6$ salts, as demonstrated in Figures S11 and S12. Therefore, for a high-voltage LCO with surface modulation, the cycle stability can be reduced when there exists some layer-type interface structure. It is far from enough to obtain an eligible high-voltage LCO via just applying surface modulations. Avoiding the GBC generation upon rolling, reinforcing the grain boundary, and/or applying single-crystal LCO may be the promise optimization strategies.

3.4. GBC Induced Structure Damage Upon Cycle. SEM, XPS, and TEM characterizations of HV-LCO and HV-LCO-15 electrodes after 200 cycles at a current of 1C are applied to reveal the GBC induced structure damage upon long-term cycles. Figure 4a, 4b shows the SEM morphology of electrodes after 200 cycles, for HV-LCO, no macroscopic cracks are observed, while for HV-LCO-15, there exists obvious cracks and macroscopic slip of Co–O planes. The result indicates that the GBC can expand gradually upon long-term cycles. XPS are further utilized to analyze the CEI compositions. By comparing the F 1s spectra of the cycled electrodes (Figure 4c), we find that the CEI of the cycled HV-LCO-15 contains more side products than the cycled HV-LCO, including $\text{Li}_x \text{PF}_y \text{O}_z$, LiF, etc., $^{39-41}$ demonstrating more serious side reactions due to the GBC generation.

Generally, the deteriorated cycle stability is closely related to the structure damage upon cycle. Herein, TEM characterizations are applied to reveal the difference between the surface and bulk structures of the cycled electrodes. Figure 4d shows TEM results of the cycled HV-LCO, in which the spinel-type interface structure in the surface region is well preserved (region A1), and the subsurface and the bulk regions (regions A2 and A3) also exhibit the original layered structure. That is to say, no essential structure changes is observed between the pristine and cycled electrodes, but the thickness of the surface spinel-type structure is slightly increased from 5 to 10 nm. This

result indicates that, an eligible high-voltage LCO cathode can be achieved if the interface structure only contains the protective spinel-type structure. For HV-LCO-15, the interface structure includes the phase structures in both surface and GBC regions. Figure 4e shows the TEM results in the surface region of cycled HV-LCO-15. The original spinel structure in surface region (region B1) is well preserved, with nearly the same thickness of about 5 nm, and the subsurface region (region B2) shows the pure layered structure. This result indicates that, the spinel-type interface structure in the surface region of HV-LCO-15 is well maintained even after 200 cycles at 4.6 V. Therefore, the acceleration of capacity decline is mainly due to the GBC generation, rather than the surface structure deterioration.

Figure 4f shows the TEM results near the GBC regions of the cycled HV-LCO-15. After 200 cycles, the GBC region among the primary crystals is obviously expanded. Alternatively, the grain boundary's region has been further torn by the repeated Li⁺ extraction/insertion during long-term cycles. This result demonstrates a basic fact that once the roll-induced GBC generates, it will inevitably develop into a macroscopic cracking across the LCO particle. Besides, obvious structure changes are further detected inside the primary crystals. For a primary crystal, whether in the regions nearby the grain boundary or in the interior regions, some visible intragranular cracks are observed, accompanied by the formation of spinel phases (regions C1, C2). The accumulation of spinel phases in the primary crystals reduces the amount of Li⁺ storage sites, thus leading to the deteriorated cycle stability. Notably, the above structure damage originated from the GBC generation upon rolling is first reported in literature.

Therefore, we clarify a GBC induced capacity decline of HV-LCO-15, and the correlated mechanism diagram is shown in Figure 5. After rolled with high pressure, the GBC is inevitably generated among different primary crystals of HV-LCO. The GBC generation introduces additional layer-type interface structure in HV-LCO-15. As a result, the interface structure

alters from a pure surface spinel-type phase (HV-LCO) to hybrid phases of surface spinel plus boundary layer (HV-LCO-15), which exposes some nonprotective layer phase against the electrolyte. These exposed layer-type phase structure is not durable enough to tolerate the repeated Li+ extraction/ insertion, thus leading to the serious bulk structure damage after long-term cycles. These bulk structure damage includes expanding GBC along grain boundaries, forming intragranular cracks and electrochemical inert spinel phases in bulk regions, etc., eventually leading to the deteriorated cycle stability. Since the capacity decline of the rolled electrode is rooted from the GBC generation, strategies to reinforce the grain boundary of LCO, or applying the monocrystalline LCO cathodes are the main focus of solutions now and in the future.

4. CONCLUSIONS

In this work, we observe the GBC generation inside the rolled HV-LCO-15, and we reveal the correlation mechanism between the GBC generation and the accelerated capacity decline behavior. Some conclusive experimental results are provided to demonstrate the altered Li⁺ transport routes due to the GBC generation, mainly via analyzing the dQ/dV, CV, and TEM results. The concept of interface structure, referring to the phase structure directly in contact with the electrolyte, is proposed and emphasized to clarify the Li⁺ transport behavior. When GBC generates upon rolling, the interface structure alters from a pure surface spinel-type phase (HV-LCO) to hybrid phases of surface spinel plus boundary layer (HV-LCO-15). This alternation of Li⁺ transport routes introduces more risk of side reactions and structure damage upon long-term cycling, as demonstrated by TEM and XPS results. From a structural perspective, the GBC induced capacity decline of the rolled HV-LCO at 4.6 V is mainly due to the gradually expanded GBC upon cycle, the formation of intragranular cracks and the associated inactive spinel phase, etc. This work reveals a new viewpoint on failure mechanism of high-voltage LCO cathode and provides the guiding significance for designing the next-generation cathode materials.

ASSOCIATED CONTENT

Supporting Information

The Supporting Information is available free of charge at https://pubs.acs.org/doi/10.1021/acsami.3c09043.

> XRD patterns of C-LCO and HV-LCO; SEM image of C-LCO, HV-LCO and HV-LCO-15; XPS for HV-LCO and HV-LCO-15; HRTEM images of HV-LCO; photo of the manual hydraulic press machine; variation curves of the electrode compact density; and electrochemical data including cycling, charge/discharge curves, and dQ/ dV curves data for the prepared samples (PDF)

AUTHOR INFORMATION

Corresponding Authors

Hui Chen - School of Materials and Environmental Engineering, Shenzhen Polytechnic, Shenzhen 518055, P. R. China; Email: chenhui2022@szpt.edu.cn

Qinghe Zhao - School of Advanced Materials, Peking University Shenzhen Graduate School, Shenzhen 518055, P. R. China; Email: zhaoqh@pku.edu.cn

Feng Pan - School of Advanced Materials, Peking University Shenzhen Graduate School, Shenzhen 518055, P. R. China;

orcid.org/0000-0002-8216-1339; Email: panfeng@ pkusz.edu.cn

Authors

Haocong Yi - School of Advanced Materials, Peking University Shenzhen Graduate School, Shenzhen 518055, P.

Yuhao Du - School of Advanced Materials, Peking University Shenzhen Graduate School, Shenzhen 518055, P. R. China

Jianjun Fang - School of Advanced Materials, Peking University Shenzhen Graduate School, Shenzhen 518055, P. R. China

Zijian Li - School of Advanced Materials, Peking University Shenzhen Graduate School, Shenzhen 518055, P. R. China

Hengyu Ren – School of Advanced Materials, Peking University Shenzhen Graduate School, Shenzhen 518055, P. R. China

Wenguang Zhao - School of Advanced Materials, Peking University Shenzhen Graduate School, Shenzhen 518055, P.

Lin Zhou - School of Advanced Materials, Peking University Shenzhen Graduate School, Shenzhen 518055, P. R. China

Complete contact information is available at: https://pubs.acs.org/10.1021/acsami.3c09043

Author Contributions

Haocong Yi and Yuhao Du contributed equally to this work. **Notes**

The authors declare no competing financial interest.

ACKNOWLEDGMENTS

This work is financially supported by the National Natural Science Foundation of China (52102201), and the Basic and Applied Basic Research Foundation of Guangdong Province (No. 2021B1515130002).

REFERENCES

(1) Lyu, Y.; Wu, X.; Wang, K.; Feng, Z.; Cheng, T.; Liu, Y.; Wang, M.; Chen, R.; Xu, L.; Zhou, J.; Lu, Y.; Guo, B. An Overview on the Advances of LiCoO₂ Cathodes for Lithium-Ion Batteries. Adv. Energy Mater. 2021, 11 (2), 2000982.

(2) Hu, E.; Li, Q.; Wang, X.; Meng, F.; Liu, J.; Zhang, J.-N.; Page, K.; Xu, W.; Gu, L.; Xiao, R.; Li, H.; Huang, X.; Chen, L.; Yang, W.; Yu, X.; Yang, X.-Q. Oxygen-redox Reactions in LiCoO₂ Cathode without O-O Bonding During Charge-discharge. Joule 2021, 5 (3), 720-736.

(3) Zhang, F.; Lou, S.; Li, S.; Yu, Z.; Liu, Q.; Dai, A.; Cao, C.; Toney, M. F.; Ge, M.; Xiao, X.; Lee, W. K.; Yao, Y.; Deng, J.; Liu, T.; Tang, Y.; Yin, G.; Lu, J.; Su, D.; Wang, J. Surface Regulation Enables High Stability of Single-crystal Lithium-ion Cathodes at High Voltage. Nat. Commun. 2020, 11 (1), 3050.

(4) Merryweather, A. J.; Schnedermann, C.; Jacquet, Q.; Grey, C. P.; Rao, A. Operando Optical Tracking of Single-particle Ion Dynamics in Batteries. Nature 2021, 594 (7864), 522-528.

(5) Li, J.; Ji, Y.; Song, H.; Chen, S.; Ding, S.; Zhang, B.; Yang, L.; Song, Y.; Pan, F. Insights Into the Interfacial Degradation of High-Voltage All-Solid-State Lithium Batteries. Nanomicro Lett. 2022, 14 (1), 191.

(6) Xu, J. Critical Review on Cathode-electrolyte Interphase Toward High-Voltage Cathodes for Li-Ion Batteries. Nanomicro Lett. 2022, 14 (1), 166.

(7) Li, J.; Lin, C.; Weng, M.; Qiu, Y.; Chen, P.; Yang, K.; Huang, W.; Hong, Y.; Li, J.; Zhang, M.; Dong, C.; Zhao, W.; Xu, Z.; Wang, X.; Xu, K.; Sun, J.; Pan, F. Structural Origin of the High-voltage Instability of Lithium Cobalt Oxide. Nat. Nanotechnol 2021, 16 (5), 599-605.

- (8) Huang, W.; Zhao, Q.; Zhang, M.; Xu, S.; Xue, H.; Zhu, C.; Fang, J.; Zhao, W.; Ren, G.; Qin, R.; Zhao, Q.; Chen, H.; Pan, F. Surface Design with Cation and Anion Dual Gradient Stabilizes High-Voltage LiCoO₂. Adv. Energy Mater. **2022**, 12 (20), 2200813.
- (9) Xu, S.; Tan, X.; Ding, W.; Ren, W.; Zhao, Q.; Huang, W.; Liu, J.; Qi, R.; Zhang, Y.; Yang, J.; Zuo, C.; Ji, H.; Ren, H.; Cao, B.; Xue, H.; Gao, Z.; Yi, H.; Zhao, W.; Xiao, Y.; Zhao, Q.; Zhang, M.; Pan, F. Promoting Surface Electric Conductivity for High-Rate LiCoO₂. Angew. Chem., Int. Ed. Engl. 2023, 62 (10), No. e202218595.
- (10) Ren, H.; Zhao, W.; Yi, H.; Chen, Z.; Ji, H.; Jun, Q.; Ding, W.; Li, Z.; Shang, M.; Fang, J.; Li, K.; Zhang, M.; Li, S.; Zhao, Q.; Pan, F. One-Step Sintering Synthesis Achieving Multiple Structure Modulations for High-Voltage LiCoO₂. Adv. Funct. Mater. **2023**, 2302622.
- (11) Dong, W.; Ye, B.; Cai, M.; Bai, Y.; Xie, M.; Sun, X.; Lv, Z.; Huang, F. Superwettable High-Voltage LiCoO₂ for Low-Temperature Lithium Ion Batteries. *ACS Energy Lett.* **2023**, 8 (2), 881–888.
- (12) Yang, X.; Wang, C.; Yan, P.; Jiao, T.; Hao, J.; Jiang, Y.; Ren, F.; Zhang, W.; Zheng, J.; Cheng, Y.; Wang, X.; Yang, W.; Zhu, J.; Pan, S.; Lin, M.; Zeng, L.; Gong, Z.; Li, J.; Yang, Y. Pushing Lithium Cobalt Oxides to 4.7 V by Lattice-Matched Interfacial Engineering. *Adv. Energy Mater.* **2022**, 12 (23), 2200197.
- (13) Fan, T.; Wang, Y.; Harika, V. K.; Nimkar, A.; Wang, K.; Liu, X.; Wang, M.; Xu, L.; Elias, Y.; Sclar, H.; Chae, M. S.; Min, Y.; Lu, Y.; Shpigel, N.; Aurbach, D. Highly Stable 4.6 V LiCoO₂ Cathodes for Rechargeable Li Batteries by Rubidium-Based Surface Modifications. *Adv. Sci. (Weinh)* **2022**, *9* (33), 2202627.
- (14) Qian, J.; Liu, L.; Yang, J.; Li, S.; Wang, X.; Zhuang, H. L.; Lu, Y. Electrochemical Surface Passivation of LiCoO₂ Particles at Ultrahigh Voltage and Its Applications in Lithium-based Batteries. *Nat. Commun.* **2018**, *9* (1), 4918.
- (15) Wang, X.; Wu, Q.; Li, S.; Tong, Z.; Wang, D.; Zhuang, H. L.; Wang, X.; Lu, Y. Lithium-Aluminum-Phosphate Coating Enables Stable 4.6 V Cycling Performance of LiCoO₂ at Room Temperature and Beyond. *Energy Storage Materials* **2021**, *37*, 67–76.
- (16) Mao, S.; Shen, Z.; Zhang, W.; Wu, Q.; Wang, Z.; Lu, Y. Outside-In Nanostructure Fabricated on LiCoO₂ Surface for High-Voltage Lithium-Ion Batteries. *Adv. Sci.* (Weinh) **2022**, 9 (11), 2104841.
- (17) Zhu, Z.; Yu, D.; Shi, Z.; Gao, R.; Xiao, X.; Waluyo, I.; Ge, M.; Dong, Y.; Xue, W.; Xu, G.; Lee, W.-K.; Hunt, A.; Li, J. Gradientmorph LiCoO₂ Single Crystals with Stabilized Energy Density Above 3400 WhL⁻¹. *Energy Environ. Sci.* **2020**, *13* (6), 1865–1878.
- (18) Xiao, J.; Shi, F.; Glossmann, T.; Burnett, C.; Liu, Z. From Laboratory Innovations to Materials Manufacturing For Lithium-based Batteries. *Nature Energy* **2023**, 8 (4), 329–339.
- (19) Abdollahifar, M.; Cavers, H.; Scheffler, S.; Diener, A.; Lippke, M.; Kwade, A. Insights into Influencing Electrode Calendering on the Battery Performance. *Adv. Energy Mater.* **2023**, 2300973.
- (20) Wilson, J. R.; Cronin, J. S.; Barnett, S. A.; Harris, S. J. Measurement of Three-dimensional Microstructure in a LiCoO₂ Positive Electrode. *J. Power Sources* **2011**, *196* (7), 3443–3447.
- (21) Wang, C. M.; Yi, Y. B.; Sastry, A. M.; Shim, J.; Striebel, K. A. Particle Compression and Conductivity in Li-Ion Anodes with Graphite Additives. *J. Electrochem. Soc.* **2004**, *151*, A1489—A1498.
- (22) Jiang, Y.; Yan, P.; Yu, M.; Li, J.; Jiao, H.; Zhou, B.; Sui, M. Atomistic Mechanism of Cracking Degradation at Twin Boundary of LiCoO₂. *Nano Energy* **2020**, *78*, 105364.
- (23) Yan, P.; Zheng, J.; Gu, M.; Xiao, J.; Zhang, J. G.; Wang, C. M. Intragranular Cracking as a Critical Barrier for High-voltage Usage of Layer-structured Cathode for Lithium-ion Batteries. *Nat. Commun.* **2017**, *8*, 14101.
- (24) Yaqoob, N.; Mücke, R.; Guillon, O.; Kaghazchi, P. Delithiation-induced Oxygen Vacancy Formation Increases Microcracking of LiCoO₂ Cathodes. *J. Power Sources* **2022**, *533*, 231316.
- (25) Kikkawa, J.; Terada, S.; Gunji, A.; Nagai, T.; Kurashima, K.; Kimoto, K. Chemical States of Overcharged LiCoO₂ Particle Surfaces and Interiors Observed Using Electron Energy-Loss Spectroscopy. *J. Phys. Chem. C* **2015**, *119* (28), 15823–15830.

- (26) Hitt, A.; Wang, F.; Li, Z.; Ge, M.; Zhang, Y.; Savsatli, Y.; Xiao, X.; Lee, W.-K.; Stephens, R.; Tang, M. Nanotomographic Observation and Statistical Analysis of Overcharging Induced Cracks in LiCoO₂ Single Crystalline Particles. *Energy Storage Materials* **2022**, *52*, 320–328.
- (27) Verdier, S.; El Ouatani, L.; Dedryvere, R.; Bonhomme, F.; Biensan, P.; Gonbeau, D. XPS Study on Al₂O₃- and AlPO₄-Coated LiCoO₂ Cathode Material for High-Capacity Li Ion Batteries. *J. Electrochem. Soc.* **2007**, *154*, A1088–A1099.
- (28) Huang, Y.; Zhu, Y.; Fu, H.; Ou, M.; Hu, C.; Yu, S.; Hu, Z.; Chen, C. T.; Jiang, G.; Gu, H.; Lin, H.; Luo, W.; Huang, Y. Mg-Pillared LiCoO₂: Towards Stable Cycling at 4.6 V. *Angew. Chem., Int. Ed.* **2021**, 60 (9), 4682–4688.
- (29) Wang, L.; Ma, J.; Wang, C.; Yu, X.; Liu, R.; Jiang, F.; Sun, X.; Du, A.; Zhou, X.; Cui, G. A Novel Bifunctional Self-Stabilized Strategy Enabling 4.6 V LiCoO₂ with Excellent Long-Term Cyclability and High-Rate Capability. *Advanced Science* **2019**, 6 (12), 1900355.
- (30) Hong, Y.-S.; Huang, X.; Wei, C.; Wang, J.; Zhang, J.-N.; Yan, H.; Chu, Y. S.; Pianetta, P.; Xiao, R.; Yu, X.; Liu, Y.; Li, H. Hierarchical Defect Engineering for LiCoO₂ through Low-Solubility Trace Element Doping. *Chem.* **2020**, *6* (10), 2759–2769.
- (31) Zhang, J.; Wang, P. F.; Bai, P.; Wan, H.; Liu, S.; Hou, S.; Pu, X.; Xia, J.; Zhang, W.; Wang, Z.; Nan, B.; Zhang, X.; Xu, J.; Wang, C. Interfacial Design for a 4.6 V High-Voltage Single-Crystalline LiCoO₂ Cathode. *Adv. Mater.* **2022**, *34* (8), 2108353.
- (32) Wang, Y.; Zhang, Q.; Xue, Z. C.; Yang, L.; Wang, J.; Meng, F.; Li, Q.; Pan, H.; Zhang, J. N.; Jiang, Z.; Yang, W.; Yu, X.; Gu, L.; Li, H. An In Situ Formed Surface Coating Layer Enabling LiCoO₂ with Stable 4.6 V High-Voltage Cycle Performances. *Adv. Energy Mater.* **2020**, *10* (28), 2001413.
- (33) Zhu, Z.; Wang, H.; Li, Y.; Gao, R.; Xiao, X.; Yu, Q.; Wang, C.; Waluyo, I.; Ding, J.; Hunt, A.; Li, J. A Surface Se-Substituted $\text{LiCo}[O_{2-\delta}Se_{\delta}]$ Cathode with Ultrastable High-Voltage Cycling in Pouch Full-Cells. *Adv. Mater.* **2020**, 32 (50), 2005182.
- (34) Zeng, C.; Duan, C.; Guo, Z.; Liu, Z.; Dou, S.; Yuan, Q.; Liu, P.; Zhang, J.; Luo, J.; Liu, W.; Zhang, J.; Chen, Y.; Hu, W. Ultrafastly Activated Needle Coke as Electrode Material for Supercapacitors. *Progress in Natural Science: Materials International* **2022**, 32 (6), 786–792.
- (35) Guo, Z.; Qian, G.; Wang, C.; Zhang, G.; Yin, R.; Liu, W.-D.; Liu, R.; Chen, Y. Progress in Electrode Materials for the Industrialization of Sodium-ion Batteries. *Progress in Natural Science: Materials International* **2023**, 33 (1), 1–7.
- (36) Elgrishi, N.; Rountree, K. J.; McCarthy, B. D.; Rountree, E. S.; Eisenhart, T. T.; Dempsey, J. L. A Practical Beginner's Guide to Cyclic Voltammetry. *J. Chem. Educ.* **2018**, 95 (2), 197–206.
- (37) Bard, A. J.; Faulkner, L. R. Electrochemical Methods: Fundamentals and Applications, 2nd ed.; John Wiley & Sons: Hoboken, 2001; Vol. 2, pp 580–632.
- (38) Savéant, J.-M. Elements of Molecular and Biomolecular Electrochemistry: An Electrochemical Approach to Electron Transfer Chemistry, 1st ed.; John Wiley & Sons: Hoboken, 2006.
- (39) Wu, S.; Lin, Y.; Xing, L.; Sun, G.; Zhou, H.; Xu, K.; Fan, W.; Yu, L.; Li, W. Stabilizing LiCoO₂/Graphite at High Voltages with an Electrolyte Additive. ACS Appl. Mater. Interfaces 2019, 11 (19), 17940–17951.
- (40) Ruan, D.; Chen, M.; Wen, X.; Li, S.; Zhou, X.; Che, Y.; Chen, J.; Xiang, W.; Li, S.; Wang, H.; Liu, X.; Li, W. In situ Constructing a Stable Interface Film on High-voltage LiCoO₂ Cathode via A Novel Electrolyte Additive. *Nano Energy* **2021**, *90*, 106535.
- (41) Sun, Z.; Zhou, H.; Luo, X.; Che, Y.; Li, W.; Xu, M. Design of a Novel Electrolyte Additive For High Voltage LiCoO₂ Cathode Lithium-ion Batteries: Lithium 4-benzonitrile Trimethyl Borate. *J. Power Sources* **2021**, *503*, 230033.